

Received October 7, 2018, accepted October 22, 2018, date of publication November 9, 2018,  
date of current version December 7, 2018.

Digital Object Identifier 10.1109/ACCESS.2018.2879713

# A Fine-Grained Analysis of Time Reversal MU-MISO Systems Over Correlated Multipath Channels With Imperfect CSI

BINGYAN HE<sup>ID</sup><sup>1</sup>, TAO SUN<sup>ID</sup><sup>2</sup>, ZHIJIN WANG<sup>ID</sup><sup>1</sup>, AND KAI SU<sup>3</sup>

<sup>1</sup>Computer Engineering College, Jimei University, Xiamen 361021, China

<sup>2</sup>Electronic Information School, Wuhan University, Wuhan 430072, China

<sup>3</sup>State Key Laboratory of Water Resources and Hydropower Engineering Science, Wuhan University, Wuhan 430072, China

Corresponding author: Tao Sun (suntao@whu.edu.cn)

This work was supported in part by the Education Department Foundation of Fujian Province under Grant JA15291, in part by the Fundamental Research Funds for the Central Universities of China under Grant 2042017kf0202, and in part by the Natural Science Foundation of Fujian Province of China under Grants 2017J01761 and 2018J01539.

**ABSTRACT** Time reversal (TR) is regarded as a potential future transmission scheme for multi-user (MU) multiple-input single-output (MISO) ultra-wideband (UWB) communication systems. In spite of TR's good performance in MU-MISO UWB systems, it suffers from performance degradation due to spatial correlation and imperfect channel-state information. In this paper, a comprehensive performance analysis of MU-MISO UWB systems with a TR pre-filter is provided. Both spatial correlation and channel estimation errors (CEE) are taken into account in the propagation channel model, and the system performance is mainly studied in terms of its effective signal-to-interference-plus-noise ratio (SINR), channel capacity, and bit error rate. The novel closed-form expressions for the average effective SINR are derived in order to characterize the influence of propagation conditions such as channel impulse response duration, spatial correlation, and CEE on TR performance metrics. The expressions reveal more precisely to us that spatial correlation and CEE have different effects on the average power of the desired signal, inter-symbol interference, and inter-user interference. Moreover, the impacts of spatial correlation and CEE on the performance of MU-MISO TR system are thoroughly investigated. In particular, the capacity loss of MU-MISO TR system due to spatial correlation and CEE is quantified and fully discussed at the end of this paper. It is shown that high spatial correlation and CEE cause a remarkable reduction in bandwidth efficiency. Finally, all theoretical results are confirmed by numerical simulations.

**INDEX TERMS** Beamforming, channel estimation errors, fine-grained analysis, spatial correlation, time reversal, UWB.

## I. INTRODUCTION

As the demand for high speed wireless services has continued to grow dramatically, the design of energy efficient and green networks has become a trend [1]–[4]. Market forecasts show exponential growth of data traffic, and approximately 95% of data traffic will come from indoor locations in the next few years [4]. In an indoor environment, radio signals often experience rich multipath propagation, which makes the design of 5G indoor communication systems even more challenging due to the severe inter-symbol interference (ISI). To resolve this problem, multiple-input multiple-output and/or complex equalization are needed at the receiver. Although the performance is satisfactory, it often results in a high cost and complexity of wireless terminals [3], [5]–[7]. TR is a

linear precoding technique, which uses the time-reversal channel impulse response to pre-filter the transmit signals. This pre-filter can fully harvest energy from the environment and focus energy in space and time on a point of interest [4], [8]. Importantly, the focusing property of TR can reduce ISI, co-channel interference and multi-access interference effectively. In addition, spatial focusing combats channel fading and maximizes delivered power to the intended receiver, saving energy of the transmitter and/or increasing channel capacity of wireless communication system. Therefore, TR offers a great potential of low-complexity energy-efficient communications for future wireless network [3], [4], [8], [9]. On the other hand, spatial focusing suggests that the system may have low probability of intercept features.

In other words, spatial focusing can improve the system security also [10]–[12]. With respect to secrecy aspects, the experimental results in [12] show that the received signal power at the eavesdropper is significantly lower compared with the power at the legitimate receiver whether the eavesdropper is located near the legitimate receiver or not [9].

Thanks to high spatial resolution, most of the works in TR has focused on ultrawideband (UWB) systems over multipath channels [8], [13]–[19], although some studies show that TR technique is suitable to conventional broadband systems as well [20], [21]. In broadband systems, the transmission bandwidth is reduced along with less scattering in the propagation channel compared with the UWB systems. When users are near to each other with less scattering signal, channels may become correlative to each other. Hence, the spatial correlation effect should not be ignored. Moreover, many channel models are based on the assumption of the perfect CSI at the transmitter [4]–[9], [20], [22]. However, in practice, it is hard to estimate the realistic CSI accurately. Furthermore, many papers as mentioned above focus only on the impact of spatial correlation or CEE to the system performance separately, or focus only on BER performance, without considering the spectral efficiency which is one of the main design purposes for any spatial multiplexing scheme. There is still a lack of system-level experimental investigation and comprehensive performance analysis of a multi-user TR-based communication system over correlated multipath channels with imperfect CSI.

In this paper, a comprehensive performance analysis of MU MISO-TR system is presented. The system model is generalized with practical considerations (i) the spatial correlation at both transmitter and user sides, and (ii) the channel estimation errors. Moreover, a number of system performance metrics, including the effective SINR at every user, channel capacity and BER are defined and evaluated. Furthermore, the more detailed derivations for the desired signal power, ISI power and IUI power are provided. Through these derivations, we find that strong correlation results in a marked increase in interference powers (i.e. ISI and IUI), but spatial correlation has no effect on the desired signal power. On the contrary, CEE monotonically reduces the desired signal power, but ISI and IUI power are independent from the effect of CEE. Additionally, we incorporate and examine quantitatively the impacts of spatial correlation and CEE to system performances to gain more comprehensive understanding of MU MISO-TR system. All the experimental results are based on Monte-Carlo simulation.

The rest of this paper is organized as follows: In Section II, the system model is formulated. The performance analysis of TR technique based on the power components of the received signal is presented in Section III. In Section IV, numerical simulation results and corresponding discussions are provided. Finally, concluding remarks are drawn in Section V.

*Notation:* E, \*, and  $\otimes$  denote expectation, discrete-time convolution, and the Kronecker product, respectively. The boldface lowercase  $\mathbf{a}$  and uppercase  $\mathbf{A}$  indicate vectors and

matrices, respectively. In addition,  $(\cdot)^T$  represents transpose of a matrix.  $|\cdot|$  and  $\|\cdot\|$  stand for the absolute value and the vector Euclidean norm, respectively. For a complex value, we denote  $\text{Re}\{\cdot\}$  as the real part. The notation  $\mathbb{C}^{m \times n}$  denotes  $m \times n$  complex matrix.

## II. SYSTEM MODEL

The block diagram for the MU MISO-TR system is depicted in Fig. 1. The system is equipped with  $M$  transmit antennas and  $N$  single-antenna users. Firstly, BS records the CIR of each links and then applies the complex-conjugated time-reversed CIR as a pre-filter to the transmitted sequence at the transmitter. Such pre-filter acting as a beamformer in the spatial domain focuses the RF power on the receiver.

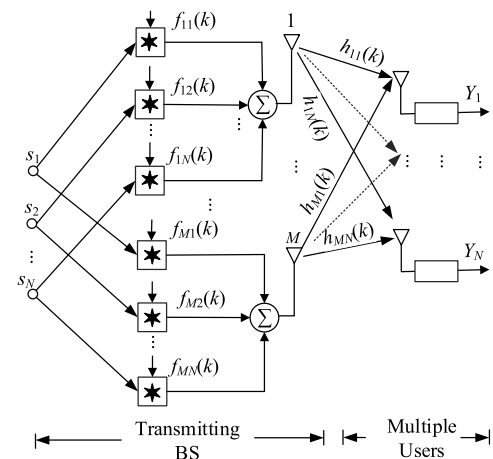


**FIGURE 1.** The diagram of multi-user MISO system using TR.

It is assumed that  $h_k(t)$  is the complex CIR, and  $h_k^*(-t)$  is the complex-conjugated time-reversed version of the CIR. Accordingly,  $h_{eq}(t) = h_k(t) * h_k^*(-t)$  is defined. When  $k = k'$ ,  $h_{eq}(t)$  is the autocorrelation function of  $h_k(t)$ , or else  $h_{eq}(t)$  is the cross-correlation function of  $h_k(t)$  and  $h_{k'}(t)$ . Importantly, the CIRs associated with different users are uncorrelated or weakly correlated and different paths of one CIR are also uncorrelated. For simplicity, we assume that a multipath channel is modeled as three fading paths, and the delays of these paths are 0,  $\tau_1$ ,  $\tau_2$ , respectively. When  $k = k'$ ,  $h_{eq}(t)$  is derived as follows

$$\begin{aligned} h_{eq}(t) &= (h_{k0}h_{k0}^* + h_{k1}h_{k1}^* + h_{k2}h_{k2}^*)\delta(t) \\ &\quad + h_{k1}h_{k0}^*\delta(t - \tau_1) + h_{k2}h_{k0}^*\delta(t - \tau_2) \\ &\quad + h_{k0}h_{k1}^*\delta(t + \tau_1) + h_{k0}h_{k2}^*\delta(t + \tau_2) \\ &\quad + h_{k1}h_{k2}^*\delta(t - \tau_1 + \tau_2) + h_{k2}h_{k1}^*\delta(t - \tau_2 + \tau_1). \end{aligned} \quad (1)$$

As shown in (1), the main lobe is strong (the first term on the right-hand side (rhs) of (1)), concentrating major part of the signal energy at the center of equivalent channel impulse response (i.e.  $t = 0$ ). This is because the peaks add up coherently as all components have zero phase here. Meanwhile, the sidelobes are minimized (the remainder except for the

first term on the rhs of (1)) as the sidelobe components are added incoherently. Therefore, the effect of ISI can be mitigated dramatically. Indeed, TR beamforming can make full use of an unavoidable but rich multipath radio propagation environment to create a spatial-temporal resonance effect and also does not require complicated channel processing and equalization. Besides, increasing the number of the transmit antennas  $M$  would contribute to enhance the focusing capability of TR.

In order to develop an analytical expression, we only consider the discrete-time signals. The maximum length of each CIR is  $L$ . The CIR from the  $i$ -th transmit antenna to the  $n$ -th user is modeled as

$$h_{in}[k] = \sum_{l=1}^L \alpha_{in,l} \delta(k - l), \quad (2)$$

where  $\alpha_{in,l}$  is the complex amplitude of the  $l$ -th tap and  $h_{in}[l] \in \mathbf{h}_{in}$ . In the following derivation process, we assume: (i) The channel coefficient at the  $l$ -th tap of the CIR ( $\alpha_{in,l}$ ) is an independent and identically distributed (i.i.d.) Gaussian random variable with the real and imaginary parts having zero mean and variance  $0.5 \sigma_{in,l}^2$  ( $E[h_{in}[l]] = 0$ ,  $E[|h_{in}[l]|^2] = \sigma_{in,l}^2$ ). (ii) Different taps of the CIR are statistically independent (uncorrelated scattering). (iii) The channel coefficients between two CIRs at the same tap index are mutually uncorrelated. Moreover, the average power of each tap decays exponentially described as  $E[|h_{in}[l]|^2] = e^{-\frac{lT}{\sigma_T^2}}$ .

Furthermore, the  $M \times N$  spatially correlated channels can be modeled as [23]

$$\mathbf{H}[k] = ((\mathbf{R}_r^{1/2})^T \otimes (\mathbf{R}_t^{1/2})) \mathbf{H}_w[k], \quad (3)$$

where  $[\mathbf{H}[k]]_{in} = h_{in}[k]$ ,  $i \in \{1 \dots M\}$ ,  $n \in \{1 \dots N\}$ , and  $k \in \{1 \dots L\}$ . The  $M \times M$  positive-define matrix  $\mathbf{R}_t$  represents the correlation between transmit antennas (the correlation coefficient  $\rho_t \in \mathbf{R}_t$ ). The  $N \times N$  positive-define matrix  $\mathbf{R}_r$  represents the correlation between different end-users (the correlation coefficient  $\rho_r \in \mathbf{R}_r$ ).  $\mathbf{H}_w[k] \in \mathbb{C}^{MN \times L}$  is the channel matrix containing the independent CIRs for a given  $k$ .

However, in a practical scenario, the true channel  $\mathbf{h}_{in}$  is not available to the transmitter. Considering the effect of CEE, the estimated CIR from the  $i$ -th transmit antenna to the  $n$ -th user can be defined as

$$\hat{\mathbf{h}}_{in} = \mathbf{h}_{in} + \mathbf{e}_{in}, \quad (4)$$

where  $h_{in}[l]$ ,  $\hat{h}_{in}[l]$  and  $e_{in}[l]$  are the true value, the estimated value, and the estimation error of the CIR, respectively. Here, the estimation errors  $\mathbf{e}_{in}$  are approximated as zero mean and i.i.d. Gaussian variables and  $\mathbf{e}_{in}$  are statistically independent of  $\mathbf{h}_{in}$  (i.e. error vector  $\mathbf{e}_{in}$  and channel vector  $\mathbf{h}_{in}$  are mutually uncorrelated). Thus, we obtain

$$E[|\hat{h}_{in}[l]|^2] = E[|h_{in}[l]|^2] + E[|e_{in}[l]|^2], \\ E[\hat{h}_{in}^*[l]h_{in}[l]] = E[|h_{in}[l]|^2].$$

Then, a error factor  $\phi$  is defined as [24]

$$E[|e_{in}[l]|^2] = \phi E[|h_{in}[l]|^2]. \quad (5)$$

Hence,  $E[|\hat{h}_{in}[l]|^2] = (1 + \phi)E[|h_{in}[l]|^2]$  can be obtained.

If the CIRs of all channels  $\hat{\mathbf{h}}_{in}$  are known at the transmitter, the pre-filter for the communication link between the  $i$ -th transmit antenna and the  $n$ -th user can be given by

$$\hat{f}_{in}[k] = \hat{h}_{in}^*[L + 1 - k] / \sqrt{\sum_{i=1}^M \sum_{l=1}^L |\hat{h}_{in}[l]|^2}. \quad (6)$$

Accordingly, the equivalent time-reversed CIR (TR-CIR) from the  $i$ -th antenna to the  $n$ -th user is formulated as

$$\hat{h}_{in}^{TR}[k] = \hat{f}_{in}[k] * h_{in}[k] \\ = \frac{\sum_{l=1}^k \hat{h}_{in}^*[L + 1 - l] h_{in}[k + 1 - l]}{\sqrt{\sum_{i=1}^M \sum_{l=1}^L |\hat{h}_{in}[l]|^2}} \quad (7)$$

with  $k = 1, 2, \dots, 2L - 1$ , and

$$\hat{h}_{in}^{TR}[L] = \frac{\sum_{l=1}^L |\hat{h}_{in}[l]|^2}{\sqrt{\sum_{i=1}^M \sum_{l=1}^L |\hat{h}_{in}[l]|^2}}. \quad (8)$$

Note that  $\hat{h}_{in}^{TR}[k]$  is the autocorrelation function of  $h_{in}[k]$ . When  $k = L$ ,  $\hat{h}_{in}^{TR}[k]$  correspondingly reaches to the maximum-power peak of the autocorrelation function. Therefore, the signal energy is concentrated at sample point  $L$ , and the focusing effect is achieved.

The signal received at user  $n$  is

$$y_n[k] = \sum_{i=1}^M \sum_{j=1}^N s_j[k] * \hat{f}_{ij}[k] * h_{in}[k] + n[k], \quad (9)$$

where each of  $\{s_1, s_2, \dots, s_N\}$  represents a sequence of information symbols that are independent complex random variables with zero mean and variance of  $\theta$ , and  $n[k]$  is zero mean Gaussian noise with variance of  $\sigma^2$ .

### III. PERFORMANCE ANALYSIS

Benefiting from the focusing property of TR, the one-tap receiver is used to sample the signal at the central tap (i.e.  $k = L$ ) and thus the complexity of TR systems can be significantly reduced. The symbol  $s_n[k - L]$  is estimated solely based on the observation of  $y_n[k]$ . And  $y_n[k]$  can be further separated into the desired signal, inter-symbol interference (ISI), inter-user interference (IUI) and noise. ISI power  $P_{ISI}$ , is derived here from (9) as the sum of the power in the TR-CIR at instants other than the focusing time ( $k \in \{1, \dots, 2L - 1\}, k \neq L$ ).

In a multi-user network, because of severe inter-user interference, SINR is always a crucial performance metric used to measure the extent to which a signal is corrupted. We study the effective SINR at each user and focus on the changes of the desired signal power and interference powers(i.e.  $P_{ISI}$  and  $P_{IUI}$ ) as a result of spatial correlation and CEE.

We define the average effective SINR at the  $n$ -th user  $SINR_{avg}^n$  as the ratio of the average signal power to the average interference-and-noise power, i.e.

$$SINR_{avg}^n = E \left[ \frac{P_s^n}{P_{isi}^n + P_{iui}^n + \sigma^2} \right], \quad (10)$$

$$P_s^n = \theta \left| \sum_{i=1}^M (\hat{f}_{in} * h_{in})[L] \right|^2, \quad (11)$$

$$P_{isi}^n = \theta \sum_{k=1}^{2L-1} \left| \sum_{i=1}^M (\hat{f}_{in} * h_{in})[k] \right|^2, \quad k \neq L \quad (12)$$

$$P_{iui}^n = \theta \sum_{n'=1}^N \sum_{k=1}^{2L-1} \left| \sum_{i=1}^M (\hat{f}_{in'} * h_{in})[k] \right|^2. \quad n' \neq n \quad (13)$$

The closed-form expression for (10) using multiple integration is very complex. Thus, we can rewrite it by using [25] as follows

$$SINR_{avg}^n \approx \frac{E[P_s^n]}{E[P_{isi}^n] + E[P_{iui}^n] + \sigma^2}. \quad (14)$$

Note that the expression in (10) bears difference with the expression in (14) in general. The latter can be treated as an approximation of the former quantity. Such an approximation is especially simpler and more useful when calculating the average SINR in some cases, e.g., this work, [9] and [24]. The performance of this approximation will be tested in the numerical results shown in Figure 5.

*Theorem 1:* For the multipath channels given in Section II, the expected value of each term for the average effective SINR (14) at user  $n$  can be obtained as shown in (27), (29), and (32).

In the (14),  $E[P_s^n]$ ,  $E[P_{isi}^n]$ , and  $E[P_{iui}^n]$  can be obtained with the help of the useful formulations as (15)-(18). Considering the correlated channel matrix, the expectation of product of two random variables can be derived as

$$E \left[ \hat{h}_{in}[l] \hat{h}_{in'}^*[l] \right] = \hat{\sigma}_{in,l} \hat{\sigma}_{in',l} (R_t)_{ii'} (R_r)_{nn'}. \quad (15)$$

Accordingly, we also have

$$E \left[ \hat{h}_{in'}^*[L+1-l] h_{in}[k+1-l] \right] = \begin{cases} (R_r)_{nn'} \frac{\hat{\sigma}_{in,L+1-l}^2}{1+\phi}, & k=L \\ 0, & \text{otherwise.} \end{cases} \quad (16)$$

For mathematical simplification, in the following derivation process, we assume that  $\hat{\sigma}_{in',l} = \hat{\sigma}_{in,l}$ , and  $\hat{\sigma}_{in',l} = \hat{\sigma}_{in,l}$ . In addition, the following analytic expression is defined

$$\xi = \frac{1}{\left( \sum_{i=1}^M E \left[ \left\| \hat{h}_{in} \right\|^2 \right] \right)}.$$

Then, the expectation of product of four random variables which are jointly Gaussian distributed is given by [26]

$$\begin{aligned} E[X_1 X_2 X_3 X_4] &= E[X_1 X_2] E[X_3 X_4] \\ &\quad + E[X_1 X_3] E[X_2 X_4] + E[X_1 X_4] E[X_2 X_3] \\ &\quad - 2E[X_1] E[X_2] E[X_3] E[X_4]. \end{aligned} \quad (17)$$

Moreover, the expectation of the expression of  $\left| \sum_{i=1}^M (\hat{f}_{in'} * h_{in})[k] \right|^2$  is given by [12]

$$\begin{aligned} E \left[ \left| \sum_{i=1}^M (\hat{f}_{in'} * h_{in})[k] \right|^2 \right] &= \sum_{i=1}^M E \left[ \left| (\hat{f}_{in'} * h_{in})[k] \right|^2 \right] \\ &\quad + E \left[ Re \left\{ \sum_{i'=1}^M \sum_{l=1}^M (\hat{f}_{in'} * h_{in})[k] (\hat{f}_{in'}^* * h_{in})^*[k] \right\} \right]. \end{aligned} \quad (18)$$

According to (7), the first term on the rhs of (18) can be formulated as

$$\begin{aligned} E \left[ \left| (\hat{f}_{in'} * h_{in})[k] \right|^2 \right] &= \xi E \left[ \left| \sum_{l=1}^k \hat{h}_{in'}^*[L+1-l] h_{in}[k+1-l] \right|^2 \right]. \end{aligned} \quad (19)$$

Based on (18), we also have

$$\begin{aligned} E \left[ \left| \sum_{l=1}^k \hat{h}_{in'}^*[L+1-l] h_{in}[k+1-l] \right|^2 \right] &= \sum_{l=1}^k E \left| \hat{h}_{in'}^*[L+1-l] h_{in}[k+1-l] \right|^2 \\ &\quad + \sum_{l=1}^k \sum_{l'=1, l' \neq l}^k E \left[ \hat{h}_{in'}^*[L+1-l] h_{in}[k+1-l] \right. \\ &\quad \times \left. \hat{h}_{in'}^*[L+1-l'] h_{in}[k+1-l'] \right]. \end{aligned} \quad (20)$$

Then, applying (16) and (17) into (20), we obtain

$$\begin{aligned} E \left| \hat{h}_{in'}^*[L+1-l] h_{in}[k+1-l] \right|^2 &= \begin{cases} (R_r)_{nn'}^2 \left( \frac{\hat{\sigma}_{in,L+1-l}^2}{1+\phi} \right)^2 + \frac{\hat{\sigma}_{in,L+1-l}^4}{1+\phi}, & k=L \\ \frac{\hat{\sigma}_{in',L+1-l}^2 \hat{\sigma}_{in,k+1-l}^2}{1+\phi}, & \text{otherwise,} \end{cases} \end{aligned} \quad (21)$$

and

$$\begin{aligned} & E \left[ \hat{h}_{in'}^* [L+1-l] h_{in} [k+1-l] \hat{h}_{in'} [L+1-l'] h_{in}^* [k+1-l'] \right] \\ &= \begin{cases} (R_r)_{nn'}^2 \left( \hat{\sigma}_{in,L+1-l}^2 \hat{\sigma}_{in,L+1-l'}^2 \right), & k = L \\ 0, & \text{otherwise.} \end{cases} \quad (22) \end{aligned}$$

Next, the last term on the rhs of (18) can be further derived as

$$\begin{aligned} & E \left[ \operatorname{Re} \left\{ (\hat{f}_{in'} * h_{in}) [k] (\hat{f}_{i'n'} * h_{i'n})^* [k] \right\} \right] \\ &= \xi E \left\{ \sum_{l=1}^k \hat{h}_{in'}^* [L+1-l] h_{in} [k+1-l] \right. \\ & \quad \times \left. \sum_{l'=1}^k \hat{h}_{i'n'} [L+1-l'] h_{i'n}^* [k+1-l'] \right\}. \quad (23) \end{aligned}$$

When  $k = L$  and  $n' = n$ , the second term on the rhs of (23) may be expressed as

$$\begin{aligned} & E \left[ \sum_{l=1}^L \hat{h}_{in}^* [l] h_{in} [l] \sum_{l'=1}^L \hat{h}_{i'n} [l'] h_{i'n}^* [l'] \right] \\ &= E \left[ \sum_{l=1}^L (h_{in}^* [l] + e_{in}^* [l]) h_{in} [l] \sum_{l'=1}^L (h_{i'n} [l'] + e_{i'n} [l']) h_{i'n}^* [l'] \right]. \quad (24) \end{aligned}$$

Note that  $E[e_{in}^* [l] h_{in} [l]] = 0$ . Thus, we have

$$\begin{aligned} & E \left[ e_{in}^* [l] h_{in} [l] e_{i'n} [l'] h_{i'n}^* [l'] \right] \\ &= \begin{cases} \frac{\phi (R_t)_{ii'}^2}{(1+\phi)^2} \hat{\sigma}_{in,i}^2 \hat{\sigma}_{i'n,l}^2, & l = l' \\ 0, & \text{otherwise.} \end{cases} \quad (25) \end{aligned}$$

According to (11) and (18),  $P_s^n$  can be re-written as

$$\begin{aligned} & E[P_s^n] \\ &= \theta E \left[ \left| \sum_{i=1}^M (\hat{f}_{in} * h_{in}) [L] \right|^2 \right] \\ &= \theta \sum_{i=1}^M E \left[ \left| (\hat{f}_{in} * h_{in}) [L] \right|^2 \right] \\ & \quad + \theta \xi E \left[ \operatorname{Re} \left\{ \sum_{i'=1}^M \sum_{i=1}^M \sum_{l=1}^L \hat{h}_{in}^* [l] h_{in} [l] \sum_{l'=1}^L \hat{h}_{i'n} [l'] h_{i'n}^* [l'] \right\} \right]. \quad (26) \end{aligned}$$

If  $n = n'$ ,  $(R_r)_{nn'} = 1$ . Substituting (21)-(25) ( $k = L, n = n'$ ) into (26),  $E[P_s^n]$  can be formulated as

$$E[P_s^n] = \frac{\theta \sum_{i=1}^M \left( (2+\phi) \sum_{l=1}^L \hat{\sigma}_{in,l}^4 + \left( \sum_{l=1}^L \hat{\sigma}_{in,l}^2 \right)^2 \right)}{(1+\phi)^2 \sum_{i=1}^M \sum_{l=1}^L \hat{\sigma}_{in,l}^2}$$

$$+ \frac{\theta \sum_{i'=1}^M \sum_{i=1}^M \left( \sum_{l'=1}^L \sum_{l=1}^L \hat{\sigma}_{in,l}^2 \hat{\sigma}_{i'n,l'}^2 + (1+\phi) \sum_{l=1}^L \hat{\sigma}_{in,l}^4 (R_t)_{ii'}^2 \right)}{(1+\phi)^2 \sum_{i=1}^M \sum_{l=1}^L \hat{\sigma}_{in,l}^2}. \quad (27)$$

From (27), the desired signal power is inversely proportional to  $\phi$ , i.e. the desired signal power is reduced by the error of estimated channels. Moreover, only transmit correlation has slight effect on  $P_s^n$ .

Furthermore, when  $k \neq L, n' = n$ , and  $l' = l$ , the second term on the rhs of (23) may be also expressed as

$$\sum_{l=1}^k (R_t)_{ii'}^2 \left( \hat{\sigma}_{in,L+1-l}^2 \hat{\sigma}_{in,k+1-l}^2 \right). \quad (28)$$

Substituting (21) and (28) ( $k \neq L, n = n'$ ) into (12),  $E[P_{isi}^n]$  can be further derived as

$$\begin{aligned} E[P_{isi}^n] &= \theta E \left[ \sum_{\substack{k=1 \\ k \neq L}}^{2L-1} \left| \sum_{i=1}^M (\hat{f}_{in} * h_{in}) [k] \right|^2 \right] \\ &= 2\theta E \left[ \sum_{k=1}^{L-1} \left| \sum_{i=1}^M (\hat{f}_{in} * h_{in}) [k] \right|^2 \right] \\ &= 2\theta \frac{\sum_{k=1}^{L-1} \sum_{i=1}^M \left( \sum_{l=1}^k \hat{\sigma}_{in,k+1-l}^2 \hat{\sigma}_{in,L+1-l}^2 \right)}{(1+\phi) \sum_{i=1}^M \sum_{l=1}^L \hat{\sigma}_{in,l}^2} \\ & \quad + 2\theta \frac{\sum_{k=1}^{L-1} \sum_{i=1}^M \sum_{i'=1}^M \sum_{l=1}^L \sum_{l'=1}^L (R_t)_{ii'}^2 \left( \hat{\sigma}_{in,L+1-l}^2 \hat{\sigma}_{in,k+1-l}^2 \right)}{(1+\phi) \sum_{i=1}^M \sum_{l=1}^L \hat{\sigma}_{in,l}^2}. \quad (29) \end{aligned}$$

From (29), it is easy to see that only transmit correlation has significant influence on ISI power whereas inter-user correlation does not affect it. Hence, ISI power increases fast with the increase of  $(R_t)_{ii'}$ .

Similarly, when  $k = L$  and  $n \neq n'$ , the second term on the rhs of (23) is equal to

$$\begin{aligned} & = \left( \frac{1}{1+\phi} \right)^2 \sum_{l'=1}^L \sum_{l=1}^L \hat{\sigma}_{in',l} \hat{\sigma}_{in,l} \hat{\sigma}_{i'n',l'} \hat{\sigma}_{i'n,l'} (R_r)_{nn'}^2 \\ & \quad + \sum_{l'=l}^L \left( \frac{\hat{\sigma}_{in',l} \hat{\sigma}_{in,l} \hat{\sigma}_{i'n',l'} \hat{\sigma}_{i'n,l'}}{(1+\phi)^2} \right) \left( (R_r)_{nn'}^2 + (R_t)_{ii'}^2 \right). \quad (30) \end{aligned}$$

In addition, when  $k \neq L, n \neq n'$ , and  $l' = l$ , the second term on the rhs of (23) may be represented as

$$= \sum_{i=1}^k (R_t)_{ii'}^2 \left( \hat{\sigma}_{in',L+1-l} \hat{\sigma}_{i'n',L+1-l} \hat{\sigma}_{in,k+1-l} \hat{\sigma}_{i'n,k+1-l} \right). \quad (31)$$

Substituting (21), (22), (30), and (31) into (32), we will get intended result of  $E[P_{iui}^n]$ . Based on (21), (22), (30), and (31), it is worth noting that both inter-user correlation and transmit correlation have significant influence on IUI power. As spatial correlation increases, IUI power increases faster than ISI power.

$$\begin{aligned} E[P_{iui}^n] &= \theta E \left[ \sum_{\substack{n'=1 \\ n' \neq n}}^N \sum_{k=1}^{2L-1} \left| \sum_{i=1}^M (\hat{f}_{in'} * h_{in})[k] \right|^2 \right] \\ &= \theta E \left\{ \sum_{\substack{n'=1 \\ n' \neq n}}^N \sum_{k=1}^{2L-1} \left\{ \sum_{i=1}^M \left| (\hat{f}_{in'} * h_{in})[k] \right|^2 + \right. \right. \\ &\quad \left. \left. \operatorname{Re} \left[ \sum_{\substack{i'=1 \\ i' \neq i}}^M \sum_{i=1}^M (\hat{f}_{in'} * h_{in})[k] (\hat{f}_{i'n'} * h_{i'n})^*[k] \right] \right] \right\}. \end{aligned} \quad (32)$$

Based on the above formulas, one can see that the desired signal power increases linearly with the number of antennas, but the average interference powers (i.e. ISI and IUI) are independent from it, which is due to an enhanced focusing capability with multiple transmit antennas leveraging the multipaths in the environment. This will be demonstrated in the numerical results shown in Table 1. Hence, an increase in  $M$  would increase the ratio between  $P_s$  and  $P_{isi} + P_{iui} + \sigma^2$ . As a result, it would improve the BER at high SINR.

In some scenarios, we do not need to consider the inter-user interference. The usable power ratio is a parameter that will compare different scenarios through a single metric. From the received signal in (9), since there is no inter-user interference, we know that the total received power is  $P_r = P_s + P_{isi} + \sigma^2$ . Ignoring the effect of noise, the usable power ratio is defined as

$$u_{tr} = \frac{P_s^n}{P_{isi}^n}. \quad (33)$$

Moreover, we define the effective spatial focusing parameter as the ratio between the usable power at the receiver and the usable power at the unintended receiver (without considering the ISI in the signal). This parameter measures the spatial focusing ability of the TR beamforming and has been used previously in related literature, e.g. [22]. The spatial focusing parameter is calculated as

$$\eta_{tr} \cong \frac{P_s^n}{P_{un}^n}. \quad (34)$$

In addition, the desired signal power captured by the unintended receiver is equal to the power of the sample at instant  $L$  in its equivalent TR-CIR. Hence, the interference power is expressed as

$$P_{un} = \left| \sum_{i=1}^M (f_{in} * h_{in'})[L] \right|^2. \quad (35)$$

#### IV. SIMULATION EXPERIMENTS AND NUMERICAL ANALYSIS

In this section, the time compression property of TR is assessed by analyzing the CIRs under different propagation conditions. Then, numerical evaluation for the performance parameters defined in Section III are provided and discussed. The channel model is used with bandwidth ( $B$ ) = 1 GHz, the number of taps ( $L$ )  $\sim$  11 to 110, and root mean square delay spread ( $\sigma_T$ ) =  $L * 0.9 * T_s$ . Moreover, the signal to noise ratio (SNR) is normally kept at 25 dB ( $\theta = 25$  dBm for all  $n$ , and  $\sigma^2 = 0$  dBm). It is noted that  $M \times N$  MISO denotes a MISO system having  $M$  transmit antennas transmitting to  $N$  users. All results were obtained by averaging those powers over 10000 channel realizations.

##### A. TIME COMPRESSION VALIDATION TEST

Fig. 2 shows samples of the original and the equivalent amplitude of the CIR at the intended receiver (setting  $L = 110$ ). The magnitudes of CIR have been normalized to their maximum value. Clearly, the original CIR before TR shows larger delay spread. Without using the TR-based transmission, all the multipath components at each tap have power contributions to the original CIR of one transmit antenna, which leads to a significant residual ISI power. Typically, this problem can be solved with equalization method at the receiver, RAKE receivers. But this would increase computational complexity at the receiver [22]. However, as shown in Fig.2b, the equivalent CIR after TR show that the delay window over which the effective CIR is significant is reduced, and a substantial portion of signal power is aggregated at the center tap (i.e.  $k = 110$ ) of the equivalent CIR while suppressing the interference (i.e.,  $k \in \{1, 2, \dots, 219\}, k \neq 110$ ) as much as possible. This indicates that there is temporal focusing. Thanks to the temporal focusing effect, the receiver can perform a simple one-tap detection and achieve good energy efficiency. On the other hand, in Fig.2c, it can be seen that the focusing gain of TR is weakened by the CEE. According to the experimental results, CEE causes a reduction in the desired signal power, and power focalization is decreased.

##### B. BEAMFORMING PERFORMANCE PARAMETERS

The expressions of the average effective SINR,  $U_{tr}$ , and  $\eta_{tr}$  are analyzed numerically in the previous section. Fig. 3 shows these results in terms of the number of channel tap. The experiments are based on the assumption of independent channels with perfect CSI.

As shown in Fig.3, the average effective SINR,  $U_{tr}$ , and  $\eta_{tr}$  is significantly improved when the number of antennas  $M$  increases. Especially, from Fig.3b, one can see that approximately a 3 dB gain is obtained in  $U_{tr}$  as  $M$  is doubled.

On the other hand, when CIR length  $L$  increases (more taps imply more multipaths), the effective SINR and  $U_{tr}$  keep steady and are not improved. This is because  $P_s$ ,  $P_{ISI}$  and  $P_{IUI}$  synchronously increase with the number of taps. In addition, as seen in Fig.3c,  $\eta_{tr}$  is improved quickly as

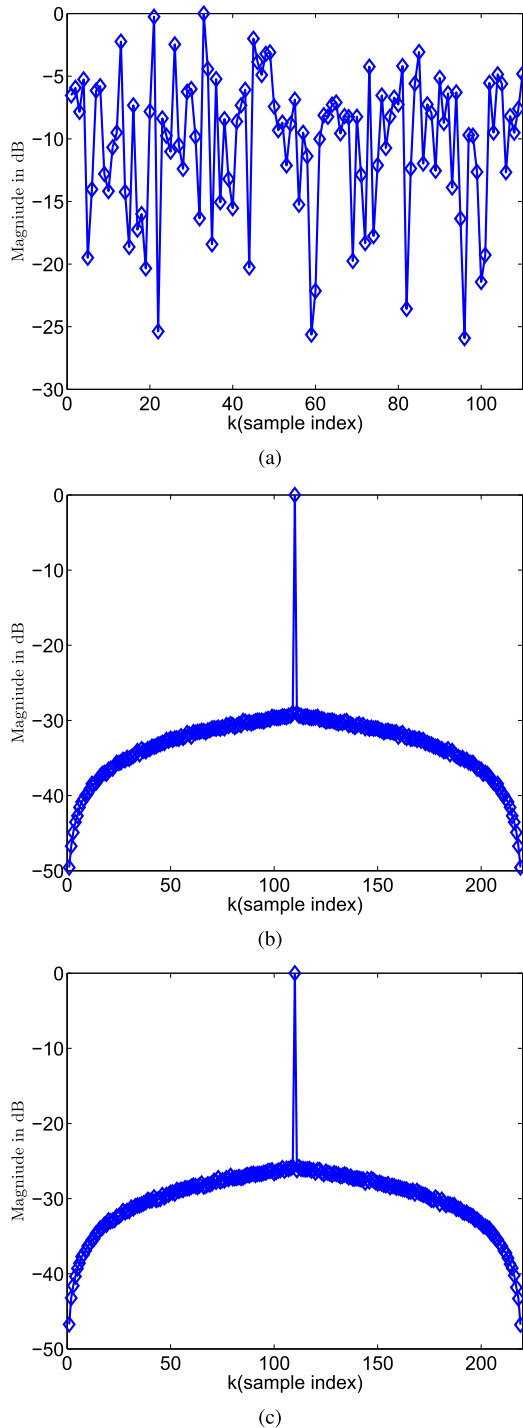


**FIGURE 2.** CIRs and temporal focusing effect obtained from experiments. (a) Original CIR obtained from one antenna without TR. (b) Equivalent CIR with TR without CEE. (c) Equivalent CIR with TR ( $\text{CEE } \phi = 0.5$ ).

more multipaths are available, which demonstrates clearly the spatial focusing properties of TR pre-coding. This is due to the increasing number of resolvable multipath components in the CIR, which are all coherently added at the intended receiver thanks to TR pre-filter. Therefore, more multipaths can improve the spatial focusing capacity of TR. Indeed, spatial focusing may be utilized in lowering co-channel

interference in multi-cell/user systems, which leads to more efficient use of the bandwidth.

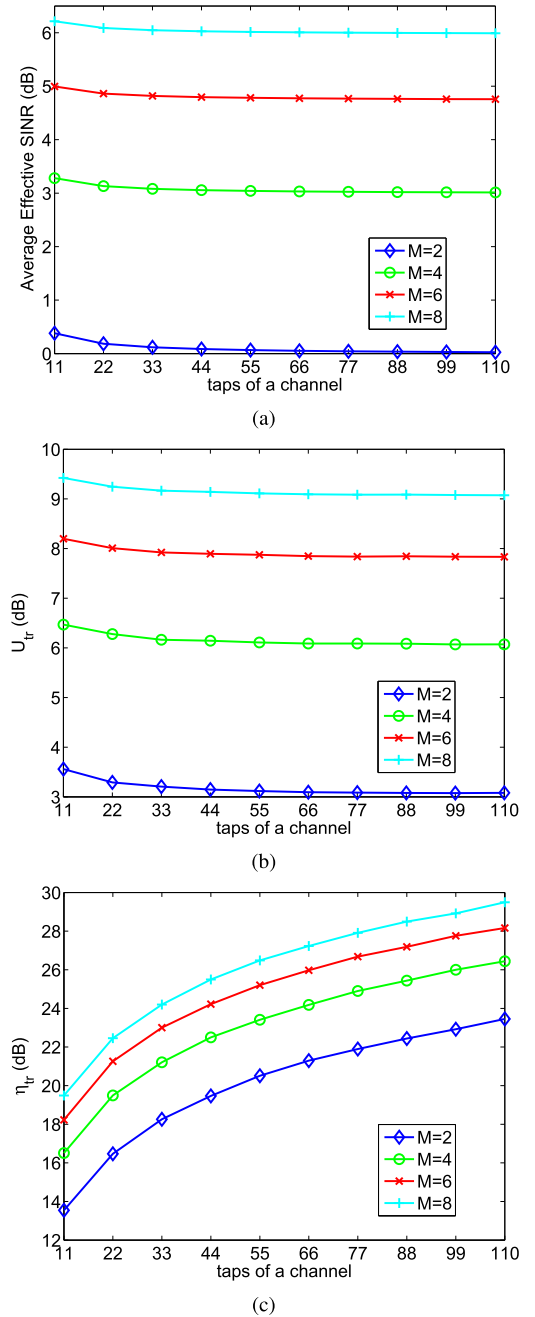


**FIGURE 3.** Performance parameters introduced in Section III. (a) effective SINR per user in multi-user network, (b) usable power ratio in the single-user case, and (c) apparent spatial focusing in multi-user network. (a) SINR versus  $L$  ( $N=2$ ).

Comparing Fig.3a with Fig.3b, it is clear that the effective SINR is far inferior to  $U_{tr}$ . Note that the calculation of SINR considers the impact of IUI in the multi-user system whereas the calculation of  $U_{tr}$  is suitable for one-user case. Fig.3a reveals that in a multi-user transmission scenario, inter-user interference can be notably severe and cause crucial performance degradation.

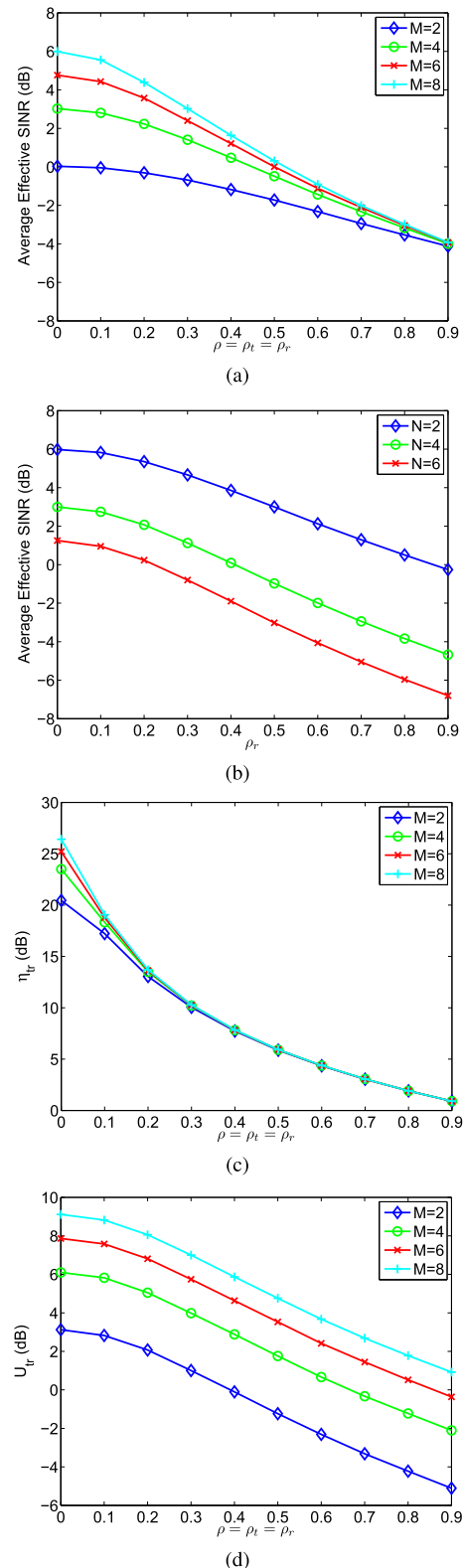


**FIGURE 4.** The effects of correlation and the number of users on performance parameters. (a) SINR versus  $\rho$ , given  $N=2$ .

Fig. 4 shows the results of the effective SINR,  $U_{tr}$ , and  $\eta_{tr}$  in terms of spatial correlation or/and the number of end-users. Note that  $\rho_t$  and  $\rho_r$  denote transmit-side correlation

coefficient and receive-side correlation coefficient, respectively. In Fig. 4, at the low correlation regime ( $\rho_t$  and  $\rho_r$  from 0 to 0.2), the more transmit antennas the system has, the better performance the system can achieve. This is because  $P_s$  increases linearly with the number of antennas whereas  $P_{ISI}$  and  $P_{IUI}$  keep constant, as listed in Table 1. But when the correlation is strong, more transmit antennas tend to result in a faster performance loss due to spatial correlation. Indeed, as shown in Fig. 4a, when  $\rho_t$  and  $\rho_r$  are greater than 0.4, the performance of the  $6 \times 2$  MISO system is already close to the performance of the  $8 \times 2$  MISO system. More antennas at the transmitter do not better the system performance.

**TABLE 1.** The effect of the number of transmit antennas.

Transmit antennas $M$	$P_s$ [dBm]	$P_{ISI}$ [dBm]	$P_{IUI}$ [dBm]
2	24.051	20.982	21.032
4	27.050	20.977	21.020
6	28.814	20.989	21.024
8	30.063	20.985	21.019

Moreover, the effective SINR,  $U_{tr}$ , and  $\eta_{tr}$  deteriorate drastically as the correlation coefficients ( $\rho_t$  and  $\rho_r$ ) increase. According to the measuring results of the numerical simulations, it is clear that significant increase in  $P_{ISI}$  and  $P_{IUI}$  causes the performance deterioration of the effective SINR,  $U_{tr}$ , and  $\eta_{tr}$ . As shown in Table 2 (the number of transmit antennas  $M = 8$ ),  $P_s$  remains unchanged whereas  $P_{ISI}$  and  $P_{IUI}$  increase significantly with increasing  $\rho$ . Obviously, when the correlation is strong, the interference cannot be mitigated effectively any more and spatial correlation degrades the focusing effect of TR.

**TABLE 2.** The impact of spatial correlation on  $P_s$ ,  $P_{ISI}$ , and  $P_{IUI}$ .

correlation coefficient $\rho_t = \rho_r$	$P_s$ [dBm]	$P_{ISI}$ [dBm]	$P_{IUI}$ [dBm]
0.0	30.063	20.985	21.019
0.1	30.068	21.285	21.642
0.2	30.066	22.064	23.068
0.3	30.058	23.098	24.727
0.4	30.063	24.243	26.337
0.5	30.068	25.373	27.780
0.6	30.065	26.441	29.083
0.7	30.071	27.433	30.233
0.8	30.072	28.354	31.261
0.9	30.096	29.234	32.221

Fig. 4b is plotted with  $M = 8$  and  $\rho_t = 0$ , demonstrating the impact of the number of users to the effective SINR at each user. Relying on the simulation results, when  $N$  increases from 2 to 4, the effective SINR per user decreases by 3 dB. Due to the IUI, more co-existing users will result in higher interference among users. That implies a tradeoff between signal reception quality at each user and the network capacity (in terms of number of serviced users). In fact, how to suppress interference effectively is still a huge challenge for the future wireless communication systems.

Furthermore, comparing the effective SINR curves ( $M = 8, N = 2$ ) in Fig. 4a and Fig. 4b, both transmit-side correlation and inter-user correlation are considered in Fig. 4a while only inter-user correlation is considered (i.e.  $\rho_t = 0$ , transmit-side correlation is not taken into account in this simulation experiment) in Fig. 4b. When  $\rho_t$  and  $\rho_r$  rise from 0 to 0.9, the effective SINR at each user decreases by 10 dB in Fig. 4a. However, when  $\rho_r$  rises from 0 to 0.9 ( $\rho_t = 0$ ), the effective SINR at each user decreases by 6 dB in Fig. 4b. This implies that double correlation will doubly degrade the performance of system. In addition, it is worth reminding that the degradation speed of the effective SINR,  $U_{tr}$ , and  $\eta_{tr}$  varies within the different ranges of  $\rho$ . In the lower range of  $\rho$  (e.g. from 0 to 0.2), the effective SINR and  $U_{tr}$  degrade slowly. On the contrary,  $\eta_{tr}$  degrades rapidly. This is due to the faster increase of  $P_{un}$ .

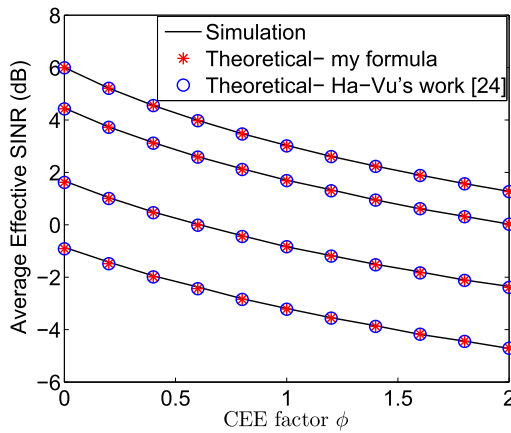


**FIGURE 5.** Effective SINR as a function of CEE and spatial correlation, given  $N = 2$ .

Fig. 5 is plotted with  $M = 8$  and  $L = 110$ , demonstrating the variation of the effective SINR vs. CEE and spatial correlation. Note that in Fig. 5, the solid curves are collected from simulations which numerically compute  $E \left[ \frac{P_s^n}{P_{isi}^n + P_{iui}^n + \sigma^2} \right]$  as shown in equation (10), and the star curves are obtained according to the analytical results given by Theorem (1). In Fig. 5, it is observed that the analytical results based on Theorem (1) are well matched with simulation results in the presence of spatial correlation and CEE, which demonstrates that equation (14) approximates well (10), and validates the effectiveness of the Theorem (1). Furthermore, the variation of the effective SINR may be seen as the function of CEE and spatial correlation. The effective SINR degrades with the increasing of CEE due to the loss of signal focalization.

### C. CHANNEL CAPACITY

Channel capacity is used as an important metric of the efficiency of a wireless downlink scheme. It presents the information rate achieved per unit bandwidth (often referred to as spectral efficiency).

For any instantaneous realization of the random channels modeled in Section II, its corresponding instantaneous

effective SINR of user  $i$  with symbol variance  $\theta$  is defined as

$$SINR(i, P/N) = \frac{P_s^n}{P_{isi}^n + P_{iui}^n + \sigma^2}, \quad (36)$$

where each term is specified in (11), (12) and (13), and the total transmit power is  $P$  ( $P = N * \theta$ ).

Then, the expected value of sum channel capacity can be obtained as

$$C_{avg} = E \left[ \varphi \sum_{i=1}^N \log_2(1 + SINR(i, P/N)) \right] (\text{bps}/\text{Hz}), \quad (37)$$

where  $\varphi$  serves as a discount factor, and  $\log_2(1 + SINR(i, P/N))$  represents the instantaneous channel capacity of user  $i$ .

In the following, without loss of generality, we use  $\varphi \approx 1$ . The numerical evaluation of the channel capacity is shown with the CIR length  $L = 110$  in the system model. The average channel capacity of every user (setting  $\varphi = 1$ ,  $\theta = 25$  dBm, and SNR = 25 dB) is plotted in Fig. 6 with different system configurations.

**TABLE 3.** Sum channel capacity comparison.

inter-user correlation $\rho_r(\rho_t = 0)$	$C_{avg}$ [bps/Hz]			
	N=2	N=4	N=8	N=16
0	4.626	6.328	7.977	9.344
0.1	4.541	6.109	7.613	8.826
0.2	4.294	5.538	6.663	7.505
0.3	3.947	4.794	5.529	6.040
0.4	3.557	4.062	4.451	4.727
0.5	3.166	3.389	3.579	3.700
0.6	2.790	2.827	2.890	2.927
0.7	2.462	2.369	2.350	2.348
0.8	2.172	1.995	1.936	1.911
0.9	1.916	1.693	1.614	1.577

As shown in Fig. 6a, the channel capacity per user increases monotonically with  $M$  in the low range of correlation, as a result of improved SINR achieved by enhanced spatial focusing. In Fig. 6b, it can be seen that even when  $\rho_t$  and  $\rho_r$  are equal to zero, a larger  $N$  (i.e. more co-existing users) degrades channel capacity of each user due to stronger interference among users, but it still gives rise to the sum channel capacity listed in Table 3. In more details, when increasing the number of co-existing users from 2 to 4 ( $\rho_t = \rho_r = 0$ ), the channel capacity per user reduces to 63% of the original while the sum channel capacity increases from 4.626 bps/Hz to 6.328 bps/Hz, i.e. the available bandwidth per user is reduced if the system serves more users. Furthermore, based on Table 3 and Fig. 6, it is observed that the more spatial correlation, the more serious IUI, there is the less the channel capacity. In fact, IUI is introduced due to the non-orthogonality of the channel impulse responses among different users. To solve this problem, signature waveform design techniques can be utilized to combat the interference. The basic idea of signature waveform design is to carefully adjust the amplitude and phase of each tap of the signature waveform based on the known CSI and thereby optimize

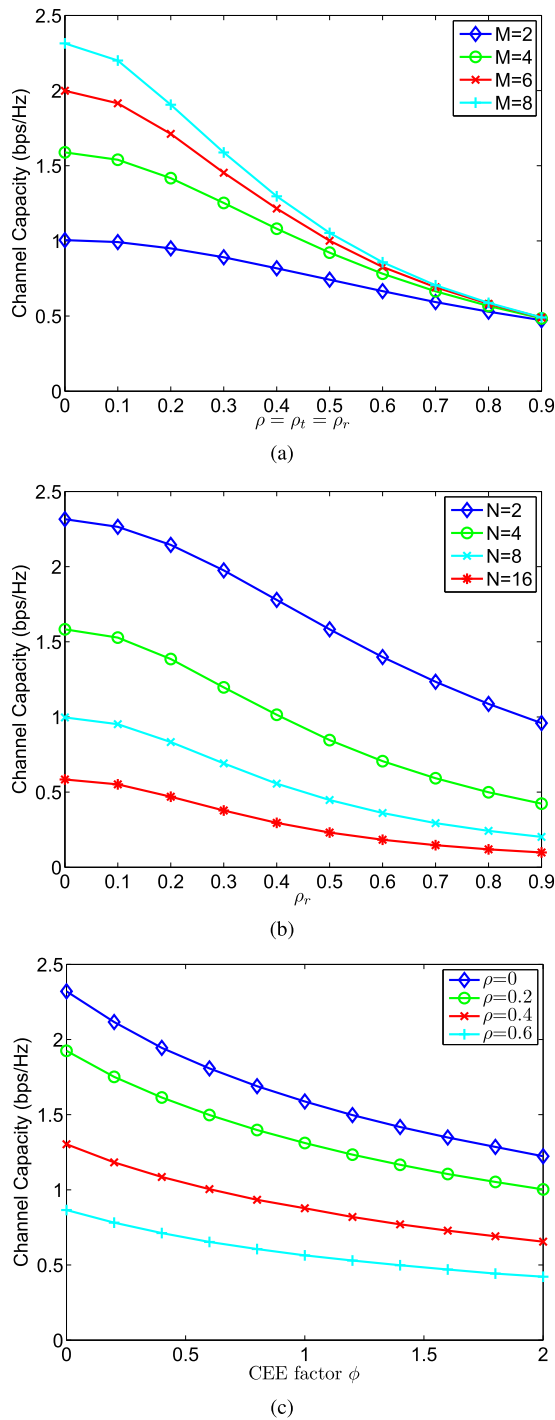


**FIGURE 6.** Channel capacity comparisons under different experimental conditions. (a) Channel capacity versus  $\rho_r$ , given  $N = 2$ . (b) Channel capacity versus #users, given  $M = 8$ . (c) Channel capacity versus CEE, given  $M = 8, N = 2$ .

the received signal to achieve low bit error rate. However, in practical systems, a mismatch between the known CSI and the true channel characteristics may occur. For example, the CSI may be outdated due to channel variations. Fig. 6c demonstrates the combined impacts of CEE and spatial correlation on channel capacity per user. It is obvious that the more errors in CSI, the less capacity is achievable.

#### D. BER PERFORMANCE

The average BER of the TR system under different channel conditions is investigated in Fig. 7. BPSK modulation is used.

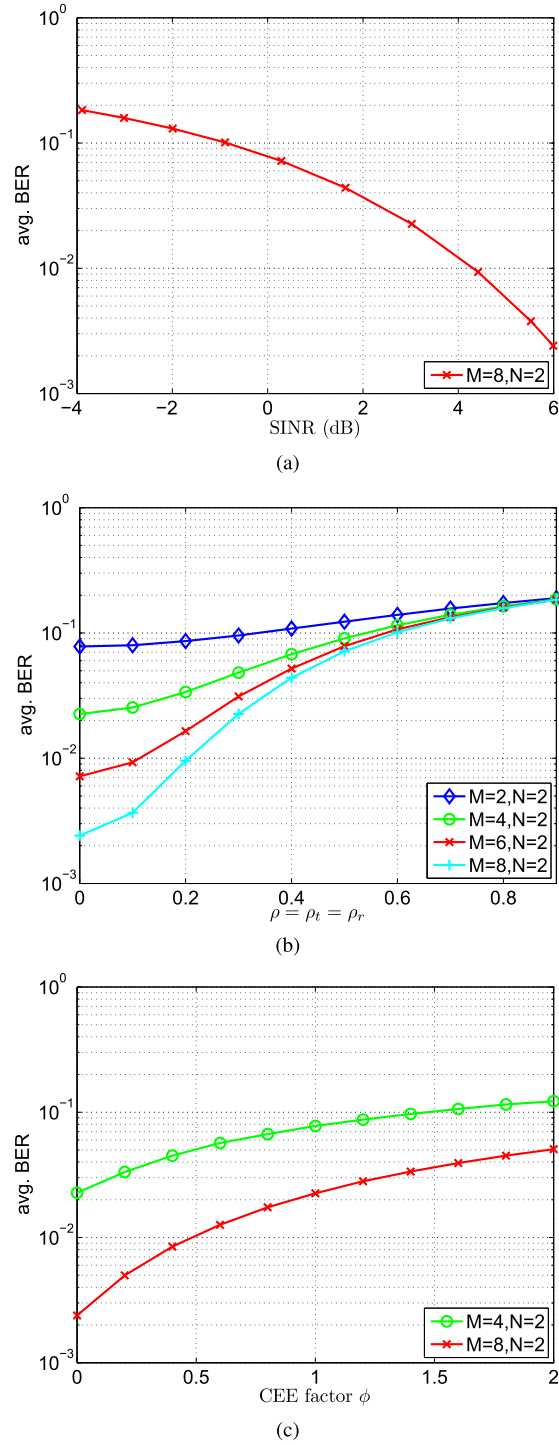


**FIGURE 7.** The impacts of CEE and spatial correlation on BER. (a) Average BER versus SINR. (b) Average BER versus  $\rho$ , given  $\phi = 0$ . (c) Average BER versus CEE, given  $\rho = 0$ .

It is worth reminding that we calculated the BER of TR as a function of SINR while keeping SNR at 25 dB.

Moreover, according to (10), (11), (12), and (13), the users can receive better SINR as transmit power scales up in low SNR regime. But in the high SNR regime where the interference power dominates the noise power, the impact of the increased interference will be more prominent and thus interference power will cause an upper bound on SINR. This is because the interference power increases as transmit power scales up. Indeed, when we increase SNR from 25 dB to 30 dB, SINR keeps stable.

Fig. 7a reveals that lower BER can be achieved at high SINR. In Fig. 7b and Fig. 7c, the effects of spatial correlation and CEE on the BER performance are tested respectively. In Fig. 7b, BER performance improves significantly as the number of antennas is doubled in the lower range of  $\rho$  (i.e. from 0 to 0.2). However, if the correlation is strong, more transmit antennas will more rapidly degrade the system performance. In addition, more errors existing in CSI also lead to the BER performance loss, but increasing the number of transmit antennas still can significantly improve the BER performance of the system, as shown in Fig. 7c.

## V. CONCLUSION

We have analyzed a TR beamforming system over correlated multipath channels with imperfect CSI. We defined and evaluated a variety of performance metrics such as the effective SINR, channel capacity and the BER. The impacts of spatial correlation and CEE on system performances were mainly studied and discussed. Also, we derived a novel closed-form approximations for the desired signal power, ISI power and IUI power.

Through theoretical analysis and simulation results, we found that TR performance is strongly dependent on propagation conditions. As observed from simulation results, more transmit antennas can improve the system performance significantly due to the transmit diversity gain at the low correlation. However, when spatial correlation is high, deploying more antennas to transmitter is unable to improve the performance of the TR system any more. Furthermore, our study demonstrates:

- Spatial correlation has negligible influence on the desired signal power, but high spatial correlation causes a rapid growth of interference powers, especially the growth of IUI power, consequently resulting in a significant deterioration in SINR performance.
- On the other hand, SINR performance is scaled down due to imperfect CSI. Actually, it is because imperfect CSI causes a reduction in desired signal power, but it does not affect ISI power and has only a slight effect on IUI power.

Hence, it is concluded that in order to get the higher obtainable performance of TR, the following conditions need to be satisfied: (i) The channels must be uncorrelated or weakly correlated so that the interference power is minimized. (ii) CEE must be minimized, therefore maximizing the desired signal power. If TR technology can be well utilized, it will yield satisfactory performance and achieve

good energy efficiency without the need for deploying complicated receivers or a large number of antennas. TR is to be a promising platform for future 5G wireless communication systems.

## REFERENCES

- [1] H.-V. Tran, G. Kaddoum, H. Tran, and E.-K. Hong, "Downlink power optimization for heterogeneous networks with time reversal-based transmission under backhaul limitation," *IEEE Access*, vol. 5, pp. 755–770, 2017.
- [2] M. Thameri, K. Abed-Meraim, F. Foroozan, R. Boyer, and A. Asif, "On the statistical resolution limit (SRL) for time-reversal based MIMO radar," *Signal Process.*, vol. 144, pp. 373–383, Mar. 2018.
- [3] L. Zou and C. Caloz, "Time-reversal routing for dispersion code multiple access (DCMA) communications," *IEEE Access*, vol. 6, pp. 9650–9654, 2018.
- [4] Y. Chen, B. Wang, Y. Han, H.-Q. Lai, Z. Safar, and K. J. R. Liu, "Why time reversal for future 5G wireless? [Perspectives]," *IEEE Signal Process. Mag.*, vol. 33, no. 2, pp. 17–26, Mar. 2016.
- [5] H. Ma, B. Wang, Y. Chen, and K. J. R. Liu, "Waveform optimizations for time-reversal cloud radio access networks," *IEEE Trans. Commun.*, vol. 66, no. 1, pp. 382–393, Jan. 2018.
- [6] Y. Han, Y. Chen, B. Wang, and K. J. R. Liu, "Realizing massive MIMO effect using a single antenna: A time-reversal approach," in *Proc. IEEE Global Commun. Conf. (GLOBECOM)*, Washington, DC, USA, Dec. 2016, pp. 1–6.
- [7] Y. Han, Y. Chen, B. Wang, and K. J. R. Liu, "Enabling heterogeneous connectivity in Internet of Things: A time-reversal approach," *IEEE Internet Things J.*, vol. 3, no. 6, pp. 1036–1047, Dec. 2016.
- [8] A. Dezfooliyan and A. M. Weiner, "Spatiotemporal focusing of phase compensation and time reversal in ultrawideband systems with limited rate feedback," *IEEE Trans. Veh. Technol.*, vol. 65, no. 4, pp. 1998–2006, Apr. 2016.
- [9] Y. Chen, Y.-H. Yang, F. Han, and K. J. R. Liu, "Time-reversal wideband communications," *IEEE Signal Process. Lett.*, vol. 20, no. 12, pp. 1219–1222, Dec. 2013.
- [10] W. Cao, J. Lei, W. Hu, and W. Li, "Secrecy capacity achievable time reversal pre-filter in MISO communication system and the unequal secrecy protection application," *Wireless Pers. Commun.*, vol. 97, no. 4, pp. 5427–5437, 2017.
- [11] H. El-Sallabi and A. Aldosari, "Characterization of secrecy capacity of time reversal technique for wireless physical layer security," in *Proc. 19th Int. Symp. Wireless Pers. Multimedia Commun. (WPMC)*, Shenzhen, China, Nov. 2016, pp. 194–198.
- [12] H.-V. Tran, H. Tran, G. Kaddoum, D.-D. Tran, and D.-B. Ha, "Effective secrecy-sinr analysis of time reversal-employed systems over correlated multi-path channel," in *Proc. IEEE 11th Int. Conf. Wireless Mobile Comput., Netw. Commun.*, Oct. 2015, pp. 527–532.
- [13] F. Maschietti, J. Fiorina, and M.-G. Di Benedetto, "Time reversal in UWB ad-hoc networks with no power control and inter-symbol interference," in *Proc. 1st Int. Conf. Future Access Enablers Ubiquitous Intell. Infrastruct. (FABULOUS)* Ohrid, Republic of Macedonia, Sep. 2015, pp. 173–180.
- [14] E. Bogdani, D. Vouyioukas, N. Nomikos, D. N. Skoutas, and C. Skianis, "Single-point model of MIMO-UWB indoor systems using time-reversal transmission," in *Proc. IEEE Int. Conf. Commun. (ICC)*, Paris, France, May 2017, pp. 1–6.
- [15] B. Fall, F. Elbahhar, M. Heddebaut, A. Rivenq, and M.-G. Di Benedetto, "Assessment of the contribution of time reversal on a UWB localization system for railway applications," *Int. J. Intell. Transp. Syst. Res.*, vol. 14, no. 3, pp. 139–151, 2016.
- [16] G. Caso, L. De Nardis, M. T. P. Le, F. Maschietti, J. Fiorina, and M.-G. Di Benedetto, "Performance evaluation of non-prefiltering vs. time reversal prefiltering in distributed and uncoordinated IR-UWB ad-hoc networks," *Mobile Netw. Appl.*, vol. 22, no. 5, pp. 796–805, 2017.
- [17] U. Zia, M. Uppal, and I. H. Naqvi, "Robust feedback design for time reversal UWB communication systems under CSIT imperfections," *IEEE Commun. Lett.*, vol. 19, no. 1, pp. 102–105, Jan. 2015.
- [18] S. M. Moghadasi and M. Dehmollaian, "Buried-object time-reversal imaging using UWB near-ground scattered fields," *IEEE Trans. Geosci. Remote Sens.*, vol. 52, no. 11, pp. 7317–7326, Nov. 2014.

- [19] D. Abbasi-Moghadam, A. Mohebbi, and Z. Mohades, "Performance analysis of time reversal UWB communication with non-coherent energy detector," *Wireless Pers. Commun.*, vol. 77, no. 3, pp. 2291–2303, 2014.
- [20] M.-A. Bouzigues, I. Siaud, M. Helard, and A.-M. Ulmer-Moll, "Turn back the clock: Time reversal for green radio communications," *IEEE Veh. Technol. Mag.*, vol. 8, no. 1, pp. 49–56, Mar. 2013.
- [21] V. Tran-Ha, D. D. Tran, D. B. Ha, and E. K. Hong, "On the performance of MU SIMO/MIMO UWB communication systems applying time-reversal technique," in *Transactions on Engineering Technologies*. Amsterdam, The Netherlands: Springer, 2014.
- [22] C. A. Viteri-Mera and F. L. Teixeira , "Equalized time reversal beamforming for frequency-selective indoor MISO channels," *IEEE Access*, vol. 5, pp. 3944–3957, 2017.
- [23] C. Oestges, "Validity of the kronecker model for MIMO correlated channels," in *Proc. 63rd IEEE Veh. Technol. Conf. (VTC Spring)*, Melbourne, VIC, Australia, May 2006, pp. 2818–2822.
- [24] H.-V. Tran, H. Nguyen, and E.-K. Hong, "Generalized analysis of MU-MISO time reversal-based systems over correlated multipath channels with estimation error," *AEU-Int. J. Electron. Commun.*, vol. 69, no. 10, pp. 1541–1549, 2015.
- [25] S. H. Rice, "A stochastic version of the price equation reveals the interplay of deterministic and stochastic processes in evolution," *BMC Evol. Biol.*, vol. 8, p. 262, Sep. 2008.
- [26] P. H. M. Janssen and P. Stoica, "On the expectation of the product of four matrix-valued Gaussian random variables," *IEEE Trans. Autom. Control*, vol. AC-33, no. 9, pp. 867–870, Sep. 1988.



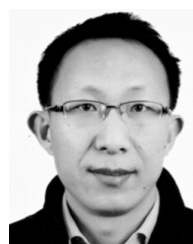
**BINGYAN HE** received the M.S. degree in electrical engineering from Wuhan University, Wuhan, in 2001. She was a Research and Development Engineer with ZTE Corporation from 2001 to 2004. She is currently with the Computer Engineering College, Jimei University, Xiamen, China. Her research interests include wireless communications, signal processing, and green communication systems.



**TAO SUN** received the Ph.D. degree in computer science in 2003. He was an Academic Visitor with the Imperial College London from 2012 to 2013. He was with the RS Group for one year. He is currently a Professor with the Electronic Information School, Wuhan University. His research fields of interest include signal processing, image processing, remote sensing image processing, computer vision, and wireless sensor networks.



**ZHIJIN WANG** received the Ph.D. degree from the Department of Computer Science and Technology, East China Normal University, Shanghai, China, in 2016. He is currently with the Computer Engineering College, Jimei University, Xiamen, China. His current research interests include recommender system, data mining, and health prediction.



**KAI SU** received the B.S. degree in hydraulic water conservancy and hydropower engineering from Former Wuhan Water Conservancy and Electric Power University, Wuhan, in 2000, and the M.S. degree and the Ph.D. degree in hydraulic water conservancy and hydropower engineering from Wuhan University, Wuhan, in 2003 and 2006, respectively. He was an Academic Visitor with the Imperial College London from 2012 to 2013. He was with the AMCG Group for one year. Since 2009, he has been an Associate Professor with Wuhan University, where he became a Professor in 2017. His majors cover hydro-mechanical interaction analysis of hydraulic structure, surrounding rock stability and support optimization of underground engineering, safety response mechanism, and regulation technology of water conveyance building.

• • •